

# Laser-Excited Luminescence of Trivalent Lanthanide Impurities and Local Structure in CeO<sub>2</sub>–ZrO<sub>2</sub> Mixed Oxides

Paolo Fornasiero,<sup>\*,†,‡</sup> Adolfo Speghini,<sup>§</sup> Roberta Di Monte,<sup>†</sup> Marco Bettinelli,<sup>\*,§</sup> Jan Kašpar,<sup>†</sup> Adriano Bigotto,<sup>†</sup> Valter Sergo,<sup>‡,||</sup> and Mauro Graziani<sup>†,‡</sup>

*Dipartimento di Scienze Chimiche, Università di Trieste and INSTM–Trieste, Via L. Giorgieri 1, I-34127 Trieste, Italy, Center of Excellence for Nanostructured Materials, Università di Trieste, Piazzale Europa 1, I-34127 Trieste, Italy, Dipartimento Scientifico e Tecnologico, Università di Verona and INSTM–Verona, Ca' Vignal, Strada Le Grazie 15, I-37134 Verona, Italy, and Dipartimento di Ingegneria dei Materiali e Chimica Applicata, Università di Trieste, Piazzale Europa 1, I-34127 Trieste, Italy*

*Received December 23, 2003. Revised Manuscript Received March 1, 2004*

In this paper we report on the laser-excited Raman and luminescence spectroscopy of a series of ceria–zirconia mixed oxides, containing trivalent lanthanide ions as unintentional impurities, using 488.0-, 514.5-, and 1064.0-nm excitation wavelengths. We assigned the main bands located at Stokes shifts higher than 800 cm<sup>-1</sup> from the laser lines to f–f emission transitions of Pr<sup>3+</sup>, Nd<sup>3+</sup>, Ho<sup>3+</sup>, and Er<sup>3+</sup> ions. These ions can also be used as spectral probes of the cation sites in the solid solutions as their transition intensities are found to be dependent on the local symmetry of the sites in which they are accommodated. f–f emission transitions have also been found to overlap the vibrational Raman bands for Stokes shifts lower than 800 cm<sup>-1</sup> from the laser lines. To overcome possible ambiguities in the structural information extracted from the Raman spectra, at least two laser excitation lines must be used.

## Introduction

Ceria–zirconia mixed oxides are extensively investigated due to their applications in the field of catalysis, particularly in the abatement of automotive emissions (three-way catalysts, TWCs).<sup>1</sup> These materials are also attractive promoters for reforming<sup>2,3</sup> and water–gas shift<sup>4</sup> reactions. Moreover, their good ionic mobility has recently opened promising perspectives for their use as solid-state conductors (e.g., in fuel cells).<sup>5,6</sup> The presence of defects due to the insertion of the smaller Zr<sup>4+</sup> ion into the CeO<sub>2</sub> lattice has been shown to play a key role in many applications of these oxide materials, as it

confers unusual properties to the mixed oxides with respect to simple materials such as CeO<sub>2</sub>.<sup>7–9</sup>

Solid-state synthesis, high-energy milling, coprecipitation, microemulsion precipitation, sol–gel synthesis, and combustion synthesis have been deeply investigated with the common target of obtaining stable single-phase ceria–zirconia solid solutions.<sup>10</sup> Therefore, the general formula Ce<sub>x</sub>Zr<sub>1–x</sub>O<sub>2</sub> is regularly used to indicate the statistical substitution of a fraction of the cerium with zirconium, in the final product. However, the homogeneity and the phase purity of the products is still a matter of debate.<sup>10</sup> This is particularly evident in the case of high surface area materials obtained for catalytic applications. In fact, the low calcination temperatures employed to obtain a high surface area sample do not allow unambiguous detection of a single-phase product. The Ce<sub>x</sub>Zr<sub>1–x</sub>O<sub>2</sub> phase diagram has been extensively studied by Yashima et al.<sup>11–13</sup> and it may be summarized as follows. Below 1273 K, for  $x > 0.85$  a cubic, fluorite-type phase c is formed (*Fm3m*), while for  $x < 0.10$ , a monoclinic phase (group *P2<sub>1</sub>/c*) is present. A

\* To whom correspondence should be addressed. Phone: +39-040-5583973. Fax: +39-040-5583903. E-mail: pforneasiero@units.it (P.F.). Phone: +39-045-8027902. Fax: +39-045-8027929. E-mail: marco.bettinelli@univ.tr (M.B.).

<sup>†</sup> Dipartimento di Scienze Chimiche, Università di Trieste and INSTM–Trieste.

<sup>‡</sup> Center of Excellence for Nanostructured Materials, Università di Trieste.

<sup>§</sup> Dipartimento Scientifico e Tecnologico, Università di Verona and INSTM–Verona.

<sup>||</sup> Dipartimento di Ingegneria dei Materiali e Chimica Applicata, Università di Trieste.

(1) Kaspar, J.; Fornasiero, P.; Graziani, M. *Catal. Today* **1999**, *50*, 285.

(2) Montoya, J. A.; Romero-Pascual, E.; Gimon, C.; Del Angel, P.; Monzon, A. *Catal. Today* **2000**, *63*, 71.

(3) Noronha, F. B.; Fendley, E. C.; Soares, R. R.; Alvarez, W. E.; Resasco, D. E. *Chem. Eng. J.* **2001**, *82*, 21.

(4) Putna, E. S.; Vohs, J. M.; Gorte, R. J. *Catal. Lett.* **1997**, *45*, 143.

(5) Kawamura, K.; Watanabe, K.; Hiramatsu, T.; Kaimai, A.; Nigara, Y.; Kawada, T.; Mizusaki, J. *Solid State Ionics* **2001**, *144*, 11.

(6) Izu, N.; Kishimoto, H.; Omata, T.; OtsukaYaoMatsuo, S. *J. Solid State Chem.* **2000**, *151*, 253.

(7) Mamontov, E.; Egami, T.; Brezny, R.; Koranne, M.; Tyagi, S. *J. Phys. Chem. B* **2000**, *104*, 11110.

(8) Sugiura, M. *Catal. Surv. Asia* **2003**, *7*, 77.

(9) Fornasiero, P.; Ranga Rao, G.; Kaspar, J.; L'Erario, F.; Graziani, M. *J. Catal.* **1998**, *175*, 269.

(10) Kaspar, J.; Fornasiero, P. *J. Solid State Chem.* **2003**, *171*, 19.

(11) Yashima, M.; Ohtake, K.; Kakihana, M.; Yoshimura, M. *J. Am. Ceram. Soc.* **1994**, *77*, 2773.

(12) Yashima, M.; Arashi, H.; Kakihana, M.; Yoshimura, M. *J. Am. Ceram. Soc.* **1994**, *77*, 1067.

(13) Yashima, M.; Takashina, H.; Kakihana, M.; Yoshimura, M. *J. Am. Ceram. Soc.* **1994**, *77*, 1869.

thermodynamically stable *t* (tetragonal,  $P4_2/nmc$ ) phase can be formed at high temperature by solid-state synthesis and upon cooling to room temperature it is obtained in the composition range  $0.10 < x < 0.30$ , while the metastable *t'* phase is observed for  $0.30 < x < 0.65$ . Finally, the *t''* or pseudo-cubic phase (also metastable) is intermediate between the *c* and *t'* phases ( $0.65 < x < 0.85$  or  $0.5 < x < 0.85$  for small particles). This is characterized by a cubic cation sublattice, while its oxygen sublattice is tetragonally distorted ( $P4_2/nmc$ ). The phase boundaries should be considered rather approximate due to the fact that, in the case of the metastable tetragonal phases, the distortion of the fluorite-type structure is highly dependent on the particle size and therefore on the thermal history of the sample. More recently, two new tetragonal phases, designated *k* and *t\**, have been reported.<sup>14,15</sup>  $ZrO_2$  is monoclinic at room temperature (space group  $P2_1/c$ ). Notably, Raman spectroscopy plays a key role in the identification of all these phases, as well as in the determination of the mechanical stress.<sup>16</sup> In fact, while powder XRD patterns are essentially determined by the arrangement of the cations (M), laser-excited Raman spectra are sensitive to M–O bonds. In addition, useful and complementary structural information can be obtained from neutron diffraction<sup>7</sup> and EXAFS data.<sup>17–22</sup> Efforts to establish a correlation between structure and reactivity of these materials have been a common approach to the majority of investigations concerning ceria–zirconia materials. Distortion in the oxygen sublattice,<sup>9,19–21</sup> highly disordered oxygens coordinated around zirconium,<sup>22</sup> formation of ordered defective pyrochlore structures,<sup>15,23,24</sup> and the presence of surface domains<sup>25,26</sup> have been invoked as justifications for the improved redox properties of  $Ce_xZr_{1-x}O_2$  with respect to  $CeO_2$ .

The presence of lanthanide ions as unavoidable impurities at the ppm or ppb level in cerium- or zirconium-based reagents is a well-known problem.<sup>27,28</sup> This is particularly evident in commercial materials,

where economic reasons limit the use of expensive high-purity reagents. However, the implications of the presence of such impurities on the structural characterization of  $Ce_xZr_{1-x}O_2$  are underestimated. In fact, laser-excited luminescence spectra of trivalent lanthanide ion impurities can superimpose to the Raman bands. These aspects become even more critical considering the fact that many lanthanide ions are used as structural dopants of ceria–zirconia solid solutions to improve redox properties,<sup>29,30</sup> surface area,<sup>31</sup> and phase stability.<sup>32</sup> For these reasons, we have found it interesting to carry out a detailed investigation of the laser-excited luminescence spectra of a series of  $Ce_xZr_{1-x}O_2$  mixed oxides, formally undoped but in fact unintentionally doped with trivalent lanthanide ion impurities. It should be noted that we decided to adopt the solid-state synthesis for the preparation of the present  $Ce_xZr_{1-x}O_2$  mixed oxides in order to obtain highly crystalline–low surface area samples, which can be structurally characterized with conventional techniques. The obtained ceramic materials are therefore more representative of electrolytes for SOFC than of catalyst components. Nevertheless, it should be underlined that the severe working conditions (peak temperature above 1273 K) of the TWC induce a strong sintering of the ceria–zirconia-based catalyst.<sup>1</sup> Therefore, the present samples could also be considered as model spent–strongly deactivated–TWC components. Further work is in progress to extend the use of laser-excited lanthanide's luminescence for the structural investigation of high surface area samples. The first aim of this study is to highlight the potential limitations in the use of single-laser excitation Raman spectroscopy for structural determination. As a second target, lanthanide ions may be utilized as valuable spectral probes<sup>33–35</sup> to obtain information about the distortion of the lattice, about the location of the lanthanide dopants, and in general on the defective structure of ceria–zirconia solid solutions. The structural information obtained from this spectroscopic tool is compared to the one previously obtained from other investigation techniques, such as XRD, Raman, and EXAFS.

## Experimental Section

Nominally undoped mixed oxides  $Ce_xZr_{1-x}O_2$  ( $x = 0, 0.10, 0.20, 0.30, 0.40, 0.50, 0.60, 0.70, 0.80, 0.90$ , and  $1.00$ ) were prepared by solid-state synthesis, by firing at 1873 K for 1 h a mixture of powders of reagent-grade  $CeO_2$  (Medolla) and  $ZrO_2$  (Hartshaw 102) in appropriate ratios. X-ray fluorescence analysis was unable to detect the presence of lanthanide impurities. Structural characterization was previously performed by powder XRD and EXAFS.<sup>20,36</sup>

(14) Kishimoto, H.; Omata, T.; Otsuka-Yao-Matsuo, S.; Ueda, K.; Hosono, H.; Kawazoe, H. *J. Alloys Compd.* **2000**, *312*, 94.

(15) Otsuka-Yao-Matsuo, S.; Omata, T.; Izu, N.; Kishimoto, H. *J. Solid State Chem.* **1998**, *138*, 47.

(16) Tomaszewski, H.; Strzeszewski, J.; Adamowicz, L.; Sergo, V. *J. Am. Ceram. Soc.* **2002**, *85*, 2855.

(17) Mastelaro, V. R.; Briois, V.; de Souza, D. P. F.; Silva, C. L. *J. Eur. Ceram. Soc.* **2003**, *23*, 273.

(18) Nagai, Y.; Yamamoto, T.; Tanaka, T.; Yoshida, S.; Nonaka, T.; Okamoto, T.; Suda, A.; Sugiura, M. *J. Synchrotron Radiat.* **2001**, *8*, 616.

(19) Fornasiero, P.; Fonda, E.; Di Monte, R.; Vlaic, G.; Kaspar, J.; Graziani, M. *J. Catal.* **1999**, *187*, 177.

(20) Vlaic, G.; Fornasiero, P.; Geremia, S.; Kaspar, J.; Graziani, M. *J. Catal.* **1997**, *168*, 386.

(21) Vlaic, G.; Di Monte, R.; Fornasiero, P.; Fonda, E.; Kaspar, J.; Graziani, M. *J. Catal.* **1999**, *182*, 378.

(22) Lemaux, S.; Bensaddik, A.; van der Eerden, A. M. J.; Bitter, J. H.; Koningsberger, D. C. *J. Phys. Chem. B* **2001**, *105*, 4810.

(23) Conesa, J. C. *J. Phys. Chem. B* **2003**, *107*, 8840.

(24) Hui, Z.; Nicolas, G.; Francoise, V.; Michele, P. *Solid State Ionics* **2003**, *160*, 317.

(25) Fornasiero, P.; Montini, T.; Graziani, M.; Kaspar, J.; Hungria, A. B.; Martinez-Arias, A.; Conesa, J. C. *Phys. Chem. Chem. Phys.* **2002**, *4*, 149.

(26) Montini, T.; Bañares, M. A.; Hickey, N.; Di Monte, R.; Fornasiero, P.; Kaspar, J.; Graziani, M. *Phys. Chem. Chem. Phys.* **2004**, *6*, 1.

(27) D'Silva, A. P.; Fessel, V. A. *Anal. Chem.* **1974**, *46*, 996.

(28) Maczka, M.; Lutz, E. T. G.; Verbeek, H. J.; Oskam, K.; Meijerink, A.; Hanuza, J.; Stuivinga, M. *J. Phys. Chem. Solids* **1999**, *60*, 1909.

(29) Bernal, S.; Blanco, G.; Cauqui, M. A.; Martin, A.; Pintado, J. M.; Galtayries, A.; Sporken, R. *Surf. Interface Anal.* **2000**, *30*, 85.

(30) Narula, C. K.; Haack, L. P.; Chun, W.; Jen, H. W.; Graham, G. W. *J. Phys. Chem. B* **1999**, *103*, 3634.

(31) Bernal, S.; Blanco, G.; Cifredo, G. A.; Perez-Omil, J. A.; Pintado, J. M.; Rodriguez-Izquierdo, J. M. *J. Alloys Compd.* **1997**, *250*, 449.

(32) Ananthapadmanabhan, P. V.; Venkatramani, N.; Rohatgi, V. K.; Momin, A. C.; Venkateswarlu, K. S. *J. Eur. Ceram. Soc.* **1990**, *6*, 111.

(33) Bunzli, J. C. G. *Luminescence Materials. In Lanthanide Probes in Life, Chemical and Earth Sciences, Theory and Practice*; Bunzli, J. C. G., Choppin, G. R. Eds.; Elsevier: Amsterdam, 1989; pp 219–293.

(34) Yugami, H.; Koike, A.; Ishigame, M.; Suemoto, T. *Phys. Rev. B* **1991**, *44*, 9214.

(35) Yugami, H.; Nakajima, A.; Ishigame, M.; Suemoto, T. *Phys. Rev. B* **1991**, *44*, 4862.

Room-temperature Raman and luminescence spectra in the visible and the near-infrared regions were excited at 488.0 or 514.5 nm using an Ar laser or at 1064 nm using a Nd:YAG laser. Spectra were obtained on either a Perkin-Elmer 2000 FT-Raman spectrometer with a diode-pumped YAG laser (1064 nm) and a room-temperature super InGaAs detector, using a laser power of 600 mW or a Renishaw S1000 system with an Ar ion laser (514.5 nm) operating in the backscattering geometry. In this latter case the power delivered to the sample was about 5 mW. Finally, the 488.0-nm line of an argon laser was also used to excite room-temperature spectra (exciting power of 100 mW). The scattered signal was passed through a suitable notch filter, collected with a 1-mm-diameter fiber and guided to a 0.46-m single monochromator (Jobin-Yvon) equipped with a CCD detector. A 1200 grooves  $\text{mm}^{-1}$  grating was used to collect the spectra (resolution  $\approx 0.05$  nm). For these spectra, the presence of the notch filter does not allow the detection of spectra features less than  $250\text{ cm}^{-1}$  from the laser line.

## Results and Discussion

**Lanthanide Luminescence Spectroscopy.** The Raman spectra of ceria–zirconia solid solutions reported in the open literature are generally presented showing the spectral region  $200\text{--}1000\text{ cm}^{-1}$ , where Raman active lattice phonons are expected. To the best of our knowledge, there are only a few exceptions, such as those reported in refs 37–39 where the spectral region has been extended up to  $3600\text{ cm}^{-1}$ . In these cases the appearance of unexpected bands located at Raman shifts higher than  $1000\text{ cm}^{-1}$  led to contradictory and sometimes doubtful interpretations. To fully understand both the nature of the Raman bands and the origin of the observed additional bands, we recorded the room-temperature laser-excited spectra for the nominally undoped series of  $\text{Ce}_x\text{Zr}_{1-x}\text{O}_2$  mixed oxides measured upon excitation at 488.0, 514.5, and 1064 nm (20490, 19440, and  $9398\text{ cm}^{-1}$ , respectively). The results are presented in Figures 1–3. The features located at Stokes shifts lower than  $800\text{ cm}^{-1}$  from the excitation line have been previously assigned to Raman active lattice phonons.<sup>12,21</sup> The Raman bands are only barely observable in the case of pure  $\text{ZrO}_2$  excited with  $\lambda = 488.0\text{ nm}$  due to the presence of broad emission bands which extend over great parts of the visible range and overlap and obscure the Raman peaks. These emission bands are assigned to transitions typical of the zirconia lattice.<sup>40–42</sup> It is also remarkable that the relatively sharp features characterized by a Stokes shift higher than  $800\text{ cm}^{-1}$  are clearly observed in  $\text{Ce}_x\text{Zr}_{1-x}\text{O}_2$  only for  $x$  ranging from 0 to 0.60–0.70; for  $x \geq 0.70$  their intensity appears to be vanishing. These bands are therefore typical of the zirconia-rich part of the series under investigation.

Relatively well-resolved bands with a Stokes shift higher than  $800\text{ cm}^{-1}$  from the laser excitation line have

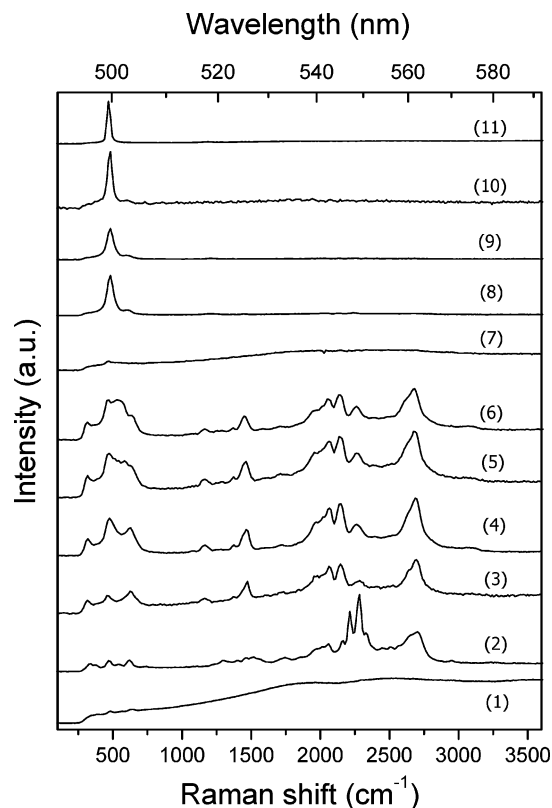


**Figure 1.** Emission spectra of  $\text{Ce}_x\text{Zr}_{1-x}\text{O}_2$  mixed oxides ( $\lambda_{\text{exc}} = 488.0\text{ nm}$ ). (1)  $\text{ZrO}_2$ , (2)  $\text{Ce}_{0.10}\text{Zr}_{0.90}\text{O}_2$ , (3)  $\text{Ce}_{0.20}\text{Zr}_{0.80}\text{O}_2$ , (4)  $\text{Ce}_{0.30}\text{Zr}_{0.70}\text{O}_2$ , (5)  $\text{Ce}_{0.40}\text{Zr}_{0.60}\text{O}_2$ , (6)  $\text{Ce}_{0.50}\text{Zr}_{0.50}\text{O}_2$ , (7)  $\text{Ce}_{0.60}\text{Zr}_{0.40}\text{O}_2$ , (8)  $\text{Ce}_{0.70}\text{Zr}_{0.30}\text{O}_2$ , (9)  $\text{Ce}_{0.80}\text{Zr}_{0.20}\text{O}_2$ , (10)  $\text{Ce}_{0.90}\text{Zr}_{0.10}\text{O}_2$ , and (11)  $\text{CeO}_2$ .

been previously observed in zirconia-based oxides and have been assigned to electronic transitions in impurity ions<sup>28</sup> or to phonon-mediated de-excitation of excited states of the impurity-doped  $\text{ZrO}_2$  lattice.<sup>43</sup> The wavelength of the features located in the visible region does not appear to shift when the incident laser wavelength changes from 488.0 to 514.5 nm; moreover, the features present in the spectrum excited at 1064 nm appear to be completely different from the ones present in the other spectra. This evidence strongly suggests that the bands having a Stokes shift higher than about  $800\text{ cm}^{-1}$  cannot be ascribed to vibrational modes and consequently must be due to electronic emission transitions. The spectral positions of these bands and their sharpness clearly indicate that they are due to f–f transitions of  $\text{Ln}^{3+}$  ions present as unintentional impurities in the material. In fact, the quantum efficiency of the luminescence from several excited states originating from the  $4f^N$  configurations is expected to be high in these mixed oxides, due to their low vibrational frequencies.<sup>44</sup> The relatively inefficient multiphonon relaxation should allow predominantly radiative emission from excited states separated by at least  $2500\text{ cm}^{-1}$  from the lower lying levels.<sup>33</sup>

This assignment agrees with recent results obtained in the case of dynamically compacted monoclinic  $\text{ZrO}_2$  in which low-level impurities of  $\text{Sm}^{3+}$  were evidenced

(36) Fornasiero, P.; Di Monte, R.; Ranga Rao, G.; Kaspar, J.; Meriani, S.; Trovarelli, A.; Graziani, M. *J. Catal.* **1995**, *151*, 168.

(37) Otake, T.; Yugami, H.; Naito, H.; Kawamura, K.; Kawada, T.; Mizusaki, J. *Solid State Ionics* **2000**, *135*, 663.

(38) Orera, V. M.; Merino, R. I.; Pena, F. *Solid State Ionics* **1994**, *72*, 224.

(39) Kaspar, J.; Fornasiero, P.; Balducci, G.; Di Monte, R.; Hickey, N.; Sergo, V. *Inorg. Chim. Acta* **2003**, *349*, 217.

(40) Pan, M.; Liu, J. R.; Yang, P.; Lu, M. K.; Xu, D.; Yuan, D. R.; Chen, D. R. *J. Mater. Sci. Lett.* **2001**, *20*, 1565.

(41) Paje, S. E.; Llopis, J. *J. Phys. Chem. Solids* **1994**, *55*, 671.

(42) Paje, S. E.; Llopis, J. *Appl. Phys. A: Mater. Sci. Process.* **1994**, *59*, 569.

(43) Asher, I. M.; Papanicolaou, B.; Anastassakis, E. *J. Phys. Chem. Solids* **1976**, *37*, 221.

(44) Blasse, G.; Grabmeier, B. C. *Luminescent Materials*; Springer: Berlin, 1994.



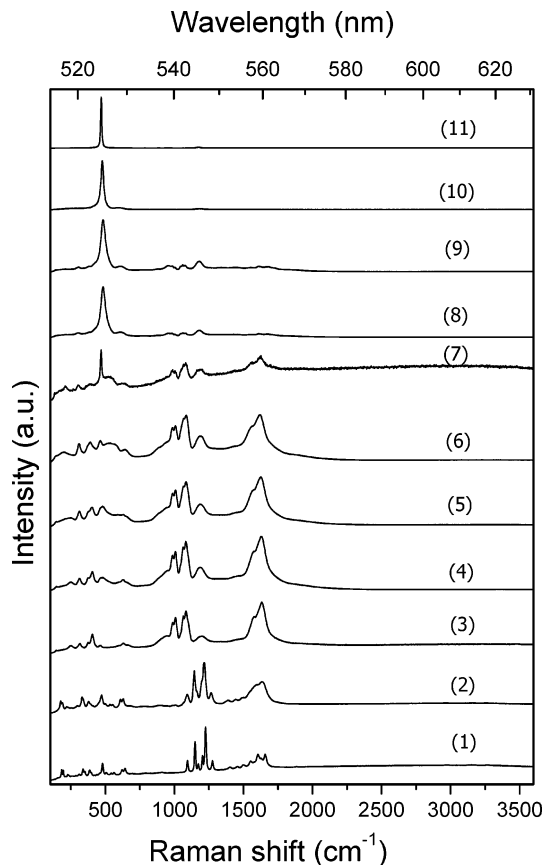


**Figure 2.** Emission spectra of  $\text{Ce}_x\text{Zr}_{1-x}\text{O}_2$  mixed oxides ( $\lambda_{\text{exc}} = 514.5 \text{ nm}$ ). (1)  $\text{ZrO}_2$ , (2)  $\text{Ce}_{0.10}\text{Zr}_{0.90}\text{O}_2$ , (3)  $\text{Ce}_{0.20}\text{Zr}_{0.80}\text{O}_2$ , (4)  $\text{Ce}_{0.30}\text{Zr}_{0.70}\text{O}_2$ , (5)  $\text{Ce}_{0.40}\text{Zr}_{0.60}\text{O}_2$ , (6)  $\text{Ce}_{0.50}\text{Zr}_{0.50}\text{O}_2$ , (7)  $\text{Ce}_{0.60}\text{Zr}_{0.40}\text{O}_2$ , (8)  $\text{Ce}_{0.70}\text{Zr}_{0.30}\text{O}_2$ , (9)  $\text{Ce}_{0.80}\text{Zr}_{0.20}\text{O}_2$ , (10)  $\text{Ce}_{0.90}\text{Zr}_{0.10}\text{O}_2$ , and (11)  $\text{CeO}_2$ .

from the visible luminescence spectra.<sup>28</sup> It must be noted that optical luminescence (albeit excited by X-rays) has already been proposed in 1974 as an analytical tool to detect low-level lanthanide impurities in  $\text{ZrO}_2$  (with detection limits 0.02–0.05 ppm). In particular, impurities of trivalent Gd, Sm, Dy, Eu, and Pr have been evidenced and quantified in nuclear-grade zirconia using this analytical procedure.<sup>27</sup>

On the basis of the well-known energy level diagram for the trivalent lanthanide ions (Figure 4) and published compilations of transition wavelengths,<sup>45,46</sup> the strongest bands above  $800 \text{ cm}^{-1}$  shown in Figures 1–3 are assigned to specific f–f transitions as reported in Table 1. In particular, the spectrum measured upon 488.0-nm excitation (Figure 1) shows sharp bands peaking at about 525, 545–550, and 560 nm, which are assigned to the transitions  $^2\text{H}_{11/2} \rightarrow ^4\text{I}_{15/2}$  of  $\text{Er}^{3+}$ , ( $^5\text{F}_4$ ,  $^5\text{S}_2$ )  $\rightarrow ^5\text{I}_8$  of  $\text{Ho}^{3+}$ , and  $^4\text{S}_{3/2} \rightarrow ^4\text{I}_{15/2}$  of  $\text{Er}^{3+}$ , respectively. In fact, the 488.0-nm incident radiation can efficiently populate the  $^4\text{F}_{7/2}$  and  $^5\text{F}_3$  excited states of  $\text{Er}^{3+}$  and  $\text{Ho}^{3+}$ , respectively; multiphonon relaxation subsequently leads to the population of the thermalized excited states ( $^2\text{H}_{11/2}$ ,  $^4\text{S}_{3/2}$ ) and ( $^5\text{F}_4$ ,  $^5\text{S}_2$ ),<sup>47,48</sup> from which emission transitions originate (Figure 4). These transitions are

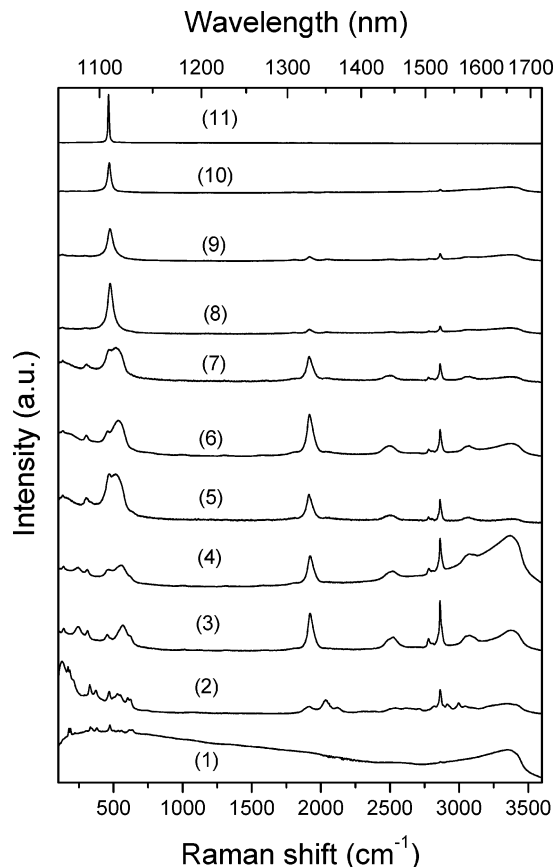


**Figure 3.** Emission spectra of  $\text{Ce}_x\text{Zr}_{1-x}\text{O}_2$  mixed oxides ( $\lambda_{\text{exc}} = 1064.0 \text{ nm}$ ). (1)  $\text{ZrO}_2$ , (2)  $\text{Ce}_{0.10}\text{Zr}_{0.90}\text{O}_2$ , (3)  $\text{Ce}_{0.20}\text{Zr}_{0.80}\text{O}_2$ , (4)  $\text{Ce}_{0.30}\text{Zr}_{0.70}\text{O}_2$ , (5)  $\text{Ce}_{0.40}\text{Zr}_{0.60}\text{O}_2$ , (6)  $\text{Ce}_{0.50}\text{Zr}_{0.50}\text{O}_2$ , (7)  $\text{Ce}_{0.60}\text{Zr}_{0.40}\text{O}_2$ , (8)  $\text{Ce}_{0.70}\text{Zr}_{0.30}\text{O}_2$ , (9)  $\text{Ce}_{0.80}\text{Zr}_{0.20}\text{O}_2$ , (10)  $\text{Ce}_{0.90}\text{Zr}_{0.10}\text{O}_2$ , and (11)  $\text{CeO}_2$ .

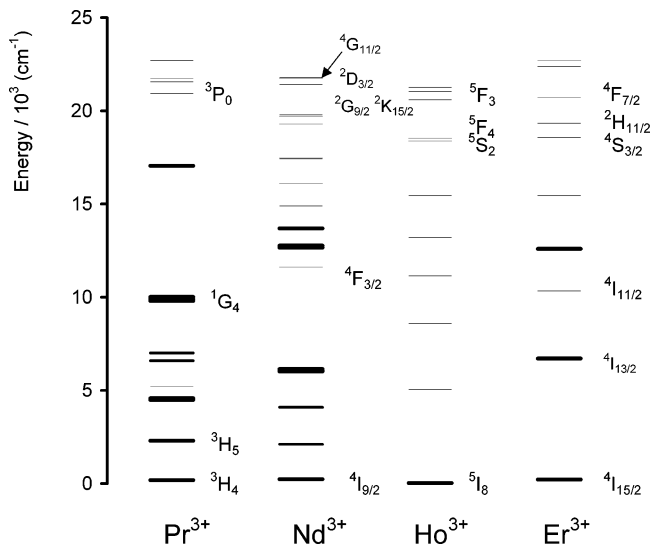


**Figure 4.** Schematic illustration of the energy levels of  $\text{Pr}^{3+}$ ,  $\text{Nd}^{3+}$ ,  $\text{Ho}^{3+}$ , and  $\text{Er}^{3+}$  below  $23000 \text{ cm}^{-1}$ .

of electric dipole origin and usually dominate the luminescence spectra of these ions in solid hosts. Their intensities are given by the Judd-Ofelt theory, which imposes selection rules on the total angular momentum quantum number  $J$ , and not on the quantum numbers  $L$  and  $S$ .<sup>49</sup>

(45) Dieke, G. H. *Spectra and Energy Levels of Rare Earth Ions in Crystals*; Interscience: New York, 1968.

(46) Kaminskii, A. A. *Laser Crystals*; Springer-Verlag: Berlin, 1990.

(47) Capobianco, J. A.; Prevost, G.; Proulx, P. P.; Kabro, P.; Bettinelli, M. *Opt. Mater.* **1996**, 6, 175.

(48) Reisfeld, R.; Hormadaly, J. *J. Chem. Phys.* **1976**, 64, 3207.

(49) Peacock, R. D. *Struct. Bonding* **1975**, 22, 83.

**Table 1. Assignment of the Emission Bands in the Laser-Excited Emission Spectra of Nominally Undoped  $\text{Ce}_x\text{Zr}_{1-x}\text{O}_2$  Mixed Oxides**

$\lambda$ emission (nm)	ion	transition
525	$\text{Er}^{3+}$	$^2\text{H}_{11/2} \rightarrow ^4\text{I}_{15/2}$
545	$\text{Ho}^{3+}$	$(^3\text{F}_4, ^5\text{S}_2) \rightarrow ^5\text{I}_8$
560	$\text{Er}^{3+}$	$^4\text{S}_{3/2} \rightarrow ^4\text{I}_{15/2}$
890	$\text{Nd}^{3+}$	$^4\text{F}_{3/2} \rightarrow ^4\text{I}_{9/2}$
1330	$\text{Pr}^{3+}$	$^1\text{G}_4 \rightarrow ^3\text{H}_5$
1540	$\text{Er}^{3+}$	$^4\text{I}_{13/2} \rightarrow ^4\text{I}_{15/2}$

We note that upon 488.0-nm excitation efficient emission is also observed around 880 nm (not shown). This band is assigned to the  $^4\text{F}_{3/2} \rightarrow ^4\text{I}_{9/2}$  electric dipole transition of  $\text{Nd}^{3+}$ ; in fact, the laser incident radiation is close to absorption transitions terminating on a group of  $\text{Nd}^{3+}$  excited levels ( $^2\text{K}_{15/2}$ ,  $^2\text{G}_{9/2}$ ,  $^2\text{D}_{3/2}$ ,  $^4\text{G}_{11/2}$ ). Multiphonon relaxation then populates the  $^4\text{F}_{3/2}$  luminescent state (Figure 4).

The spectrum obtained upon excitation at 514.5 nm (Figure 2) is similar to the one shown in Figure 1, but the Raman bands overlap the  $^2\text{H}_{11/2} \rightarrow ^4\text{I}_{15/2}$  band of  $\text{Er}^{3+}$  peaking at 525 nm (see below). In this case, the incident radiation is close to the  $^4\text{I}_{15/2} \rightarrow ^2\text{H}_{11/2}$  absorption transition of  $\text{Er}^{3+}$ . On the other hand, the laser radiation is not exactly resonant with any absorption transitions of the  $\text{Ho}^{3+}$  ion, but anyway the exciting light is sufficiently absorbed, to give rise to a significant population of the upper states of the emission transitions.

The spectrum collected with excitation wavelength equal to 1064 nm is shown in Figure 3. The main peaks are located at about 1340 and 1530 nm. These features are assigned to the transitions  $^1\text{G}_4 \rightarrow ^3\text{H}_5$  of  $\text{Pr}^{3+}$  and  $^4\text{I}_{13/2} \rightarrow ^4\text{I}_{15/2}$  of  $\text{Er}^{3+}$ , respectively. In this case the incident radiation populates directly the  $^1\text{G}_4$  state of  $\text{Pr}^{3+}$  and the  $^4\text{I}_{11/2}$  state of  $\text{Er}^{3+}$ ; the latter subsequently relaxes in a nonradiative way to the lower lying  $^4\text{I}_{13/2}$  state. The two transitions identified above have both an electric dipole and a magnetic dipole character.

The luminescence spectra therefore indicate the presence of unintentional low-level  $\text{Pr}^{3+}$ ,  $\text{Nd}^{3+}$ ,  $\text{Er}^{3+}$ , and  $\text{Ho}^{3+}$  impurities in the reagents employed in the synthesis of the mixed oxides. The intensity of these features is roughly comparable to bands located below  $800\text{ cm}^{-1}$  previously assigned to Raman bands and therefore is low for emission transitions. Therefore, the impurities could be present at the ppm (or even lower) level, and this is certainly compatible with the reagents used in the synthesis. In fact, it must be noted that visible luminescence from the  $\text{Er}^{3+}$  and  $\text{Tm}^{3+}$  ions was recently observed in  $\text{Yb}^{3+}$ -doped silicate glasses, containing  $\text{Er}^{3+}$  and  $\text{Tm}^{3+}$  ions as unintentional impurities with a concentration of 3 and 10 ppm, respectively, following excitation at 975 nm.<sup>50</sup> In these conditions the emission requires an upconversion process, which in similar cases shows an efficiency  $\ll 1\%$ ,<sup>51</sup> while in the present case the luminescence follows direct excitation of the emitting levels, or of states located just above them. So  $\text{Ln}^{3+}$  ions at ppm or sub-ppm concentration can be responsible for the observed bands.

We point out that no visible emission band is attributed to the  $\text{Pr}^{3+}$  ion, despite the fact that  $\text{Pr}^{3+}$  can

give rise to visible luminescence upon 488.0-nm excitation.<sup>52</sup> This is compatible with the presence of fast nonradiative relaxation of the  $^3\text{P}_0$  state of  $\text{Pr}^{3+}$  as observed in several simple and mixed oxides.<sup>52,53</sup>

Finally, it should be mentioned the fact that the relatively low cooling rate used for the synthesis of the present materials might lead to the formation of  $\text{Ce}^{3+}$  sites, as suggested by density measurements<sup>36</sup> and by the light-blue color of the ceria-rich samples. The  $^2\text{F}_{5/2} \rightarrow ^2\text{F}_{7/2}$  electronic transition of  $\text{Ce}^{3+}$  species present in  $\text{ZrO}_2\text{--CeO}_2\text{--Y}_2\text{O}_3$  solid solutions was invoked to explain a band observed around  $2100\text{ cm}^{-1}$ <sup>37</sup> in the Raman spectrum. This band would require an electronic Raman scattering mechanism, but in the spectra of the materials under investigation we find no clear evidence for it.

**Lanthanide Ions as Spectroscopic Probes: Structural Information.** The unintentional lanthanide impurities can be used as spectroscopic probes of the cation site symmetry in the materials under investigation. In fact, the f–f transitions appear to be clearly detectable in the pure  $\text{ZrO}_2$  sample upon 514.5-nm excitation (Figure 2), indicating that the lanthanide ions are present in this starting reagent, where presumably the impurity ions substitute for  $\text{Zr}^{4+}$  in a site of low symmetry ( $C_1$ ).

However, the intensity of these bands (relative to the Raman bands) does not appear to decrease strongly with  $x$  up to  $x = 0.60\text{--}0.70$ . This clearly indicates that in the zirconia-rich mixed oxides the sites occupied by the  $\text{Ln}^{3+}$  impurities are characterized by a relatively low symmetry. In fact, the f–f electric dipole transitions are parity forbidden, and their purely electronic intensity is nonvanishing only if the point symmetry of their sites has no center of inversion. Moreover, the higher the distortion of the  $\text{Ln}^{3+}$  sites, the stronger the intensity of the f–f electric dipole transitions.<sup>33,49</sup>

As described above, for  $x \geq 0.70$ , a rather abrupt change is observed, and the f–f transition intensities drastically decrease to the point that in  $\text{CeO}_2$  no significant luminescence is detected. The presence of this abrupt change in intensity does not seem to be due only to a preferential presence of the trivalent lanthanide impurities in the  $\text{ZrO}_2$  starting reagent, rather than in  $\text{CeO}_2$ , as this would give rise to a smooth decrease of the f–f transition intensities when  $x$  increases. For this reason, we suggest that the decrease in the luminescence intensity could be due to a decrease of the electric dipole transition probability related to an abrupt increase of the  $\text{Ln}^{3+}$  site symmetry. On this basis, we propose that in the ceria-rich mixed oxides ( $x \geq 0.70$ ) the sites available for the  $\text{Ln}^{3+}$  are probably highly symmetric, and possibly similar to the  $\text{Ce}^{4+}$  sites in  $\text{CeO}_2$ , having a fluorite structure. In fact, these sites are centrosymmetric (they are of  $O_h$  symmetry in the  $Fm\bar{3}m$  space group) and therefore purely electronic electric dipole f–f transitions are forbidden. On the other hand, for  $x = 0.60\text{--}0.20$  the metal ions  $\text{Zr}^{4+}$  and  $\text{Ce}^{4+}$  are accommodated in sites having  $D_{2d}$  symmetry in the tetragonal  $P4_2/nmc$  space group; these sites are

(50) Schaudel, B.; Goldner, P.; Prassas, M.; Auzel, F. *J. Alloys Compd.* **2000**, *300*, 443.

(51) Vetrone, F.; Boyer, J. C.; Capobianco, J. A.; Speghini, A.; Bettinelli, M. *Appl. Phys. Lett.* **2002**, *80*, 1752.

(52) Del Longo, L.; Ferrari, M.; Zanghellini, E.; Bettinelli, M.; Capobianco, J. A.; Montagna, M.; Rossi, F. *J. Non-Cryst. Solids* **1998**, *231*, 178.

(53) Donega, C. D.; Meijerink, A.; Blasse, G. *J. Phys. Chem. Solids* **1995**, *56*, 673.

**Table 2. XRD and EXAFS Characterization of Nominally Undoped  $\text{Ce}_x\text{Zr}_{1-x}\text{O}_2$  Mixed Oxides from Refs 21 and 36**

X Ce <sub>x</sub> Zr <sub>1-x</sub> O <sub>2</sub>	XRD												EXAFS			
	cubic phase		tetragonal phase t'			tetragonal phase t''			monoclinic phase <sup>a</sup>							
	<i>a</i> = <i>b</i> = <i>c</i> (Å)	(%)	<i>a</i> = <i>b</i> (Å)	<i>c</i> (Å)	(%)	<i>a</i> = <i>b</i> (Å)	<i>c</i> (Å)	(%)	<i>a</i> (Å)	<i>b</i> (Å)	<i>c</i> (Å)	(%)	C.N. <sup>b</sup>	Zr–O (Å)	C.N. <sup>b</sup>	Ce–O (Å)
1.0	5.407	(100)														
0.9	5.379	(100)														
0.8	5.353	(100)											(4)	2.164	(8)	2.330
													(2)	2.329		
0.7	5.350	(100)											(4)	2.134	(8)	2.316
0.6	5.301	(100)											(2)	2.328		
													(3)	2.117	(8)	2.31
0.5			5.260	5.304	(100)								(2)	2.325		
0.4	5.298	(11)	5.224	5.284	(67)	5.142	5.241	(22)								
0.3	5.319	(6)	5.224	5.284	(17)	5.142	5.241	(77)								
0.2						5.151	5.239	(100)					(4)	2.089	(8)	2.295
													(4)	2.301		
0.1									5.333	5.210	5.172	(100)				

<sup>a</sup>  $\beta = 98.78$ . <sup>b</sup> C.N. = coordination number.

not characterized by the presence of the center of inversion and f–f electric dipole transitions in the substitutional  $\text{Ln}^{3+}$  ions can become allowed. Finally, for  $x = 0.10$ , the solid solution is monoclinic and belongs to  $P2_1/c$  space group, with metal ions in sites with  $C_1$  symmetry, which is compatible with allowed f–f electric dipole transitions for the  $\text{Ln}^{3+}$  ions. The structural behavior obtained by XRD and EXAFS<sup>21,36</sup> (Table 2) seems to be therefore in good agreement with the observed behavior of the intensities of the f–f transitions of the unintentional impurities, which can act as structural probes of the symmetry of the sites occupied by the metal ions. This conclusion is based on the assumption that the lanthanide impurities are located in sites whose symmetry positions are representative of those of the normal positions in the cationic sublattice. On the other hand, in the case of materials consisting of more than one phase, the impurities could also be preferentially concentrated in phase boundary regions. Presently, we have no evidence for this behavior, but we cannot completely rule out this possibility. However, we point out that a preferential concentration of the lanthanide ions in the phase boundary would imply a sizable interaction among them. This should be particularly evident in our highly sintered materials, with crystallite dimensions higher than 100 nm, since the contribution of the surface and therefore also of the phase boundaries is limited. Lanthanide clusterization would lead to nonradiative relaxation mechanisms of the excited states and to a significant quenching of the luminescence. The present spectra show that the luminescence is strong (for low-level impurities), and the radiative emission does not seem to be significantly quenched by ion–ion interactions.

**Presence of Luminescence in the Raman Region.** Careful inspection of Figures 1–3 shows that luminescence bands related to  $\text{Ln}^{3+}$  impurities could also be located at Raman shifts lower than  $800\text{ cm}^{-1}$  in the spectra of the mixed oxides under investigation. In fact, the spectra of pure  $\text{CeO}_2$  exhibit a sharp single band at about  $465\text{ cm}^{-1}$ , which is due to the  $F_{2g}$  Raman active mode typical of fluorite structured materials (space group  $Fm\bar{3}m$ ).<sup>54</sup> For ceria–zirconia solid solutions with cerium content above 60 mol % ( $x \geq 0.60$ ), the Raman region is still dominated by the strong band at about  $465\text{ cm}^{-1}$ , which shifts to lower frequency as the

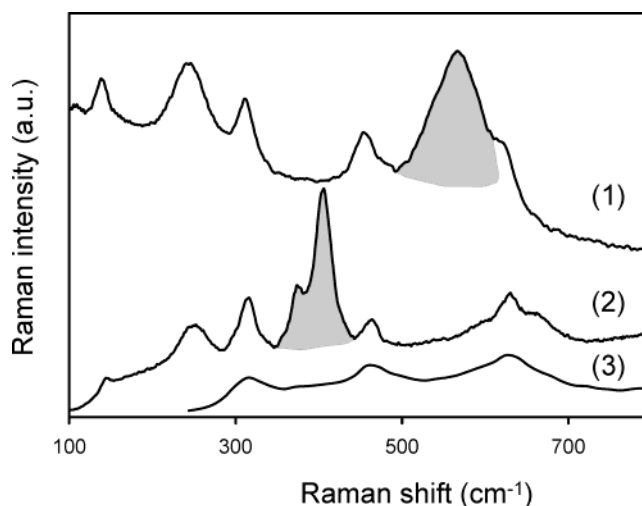


**Figure 5.** Emission spectra of  $\text{Ce}_{0.20}\text{Zr}_{0.80}\text{O}_2$  mixed oxides (trace (1) obtained with  $\lambda_{\text{exc}} = 1064.0\text{ nm}$ , trace (2) obtained with  $\lambda_{\text{exc}} = 514.5\text{ nm}$ , and trace (3) obtained with  $\lambda_{\text{exc}} = 488.0\text{ nm}$ ). Luminescence bands are highlighted in shadow.

cerium content decreases. For  $\text{Ce}_{0.20}\text{Zr}_{0.80}\text{O}_2$  and  $\text{Ce}_{0.30}\text{Zr}_{0.70}\text{O}_2$  6 bands are observed in the Raman spectra at about 137, 240, 310, 452, 590, and  $616\text{ cm}^{-1}$ , regardless of the laser excitation wavelength, as expected for a tetragonal solid solution. However, with use of the 514.5-nm line of the Argon ion laser, a strong band at  $404\text{ cm}^{-1}$  with a shoulder at  $373\text{ cm}^{-1}$  appears for the  $\text{Ce}_x\text{Zr}_{1-x}\text{O}_2$  samples having  $0.20 \leq x \leq 0.50$  (see Figure 5 as an example). These features are not present in the spectra collected using the 488.0- and 1064-nm line of the Argon and Nd:YAG lasers and therefore must be associated with luminescence. Their wavelength position (around 525 nm) is compatible with the  $^2\text{H}_{11/2} \rightarrow ^4\text{I}_{15/2}$  transition of  $\text{Er}^{3+}$ , already observed in the spectra excited at 488.0 nm (see above). Similarly, the spectra recorded using the 1064-nm line show a very strong band around  $560\text{ cm}^{-1}$  for  $0.20 \leq x \leq 0.40$  ( $512\text{ cm}^{-1}$  for the sample with  $x = 0.40$ ), which is absent in the other Raman spectra. Again, this feature has to be assigned to a luminescence transition in a  $\text{Ln}^{3+}$  impurity, whose nature has not yet been identified.

(54) Spanier, J. E.; Robinson, R. D.; Zheng, F.; Chan, S. W.; Herman, I. P. *Phys. Rev. B* **2001**, 6424, 5407.

We point out that the present  $\text{Ce}_{0.30}\text{Zr}_{0.70}\text{O}_2$  and  $\text{Ce}_{0.40}\text{Zr}_{0.60}\text{O}_2$  samples are a mixture of respectively tetragonal t phase (77 and 22%), t' phase (17 and 67%), and cubic phase (6 and 11%) (Table 2).<sup>21</sup> As already discussed, lanthanide impurities located in highly symmetric sites, such as those in the cubic phase, do not lead to luminescence bands. For the two tetragonal phases, the local symmetry around the trivalent lanthanide impurities should not be significantly different, leading to similar luminescence contribution. Therefore, the f–f transitions observed in these two samples must be considered as an average of the f–f emission from the two tetragonal phases.

The  $\text{Ce}_{0.10}\text{Zr}_{0.90}\text{O}_2$  shows major bands at 627, 609, 471, 377, 331, 208, 182, and 170  $\text{cm}^{-1}$ , which closely resemble those of pure monoclinic zirconia. Our reference monoclinic  $\text{ZrO}_2$  shows bands at 632, 613, 473, 377, 332, 218, 189, and 177  $\text{cm}^{-1}$ , which are similar to those previously observed for pure monoclinic zirconia.<sup>55–57</sup>

### Conclusions

In this paper we have analyzed and discussed the laser-excited emission spectra of a series of ceria–zirconia mixed oxides. It has been possible to assign the major bands shifted more than 800  $\text{cm}^{-1}$  from the laser excitation line to f–f emission transitions in  $\text{Pr}^{3+}$ ,  $\text{Nd}^{3+}$ ,  $\text{Ho}^{3+}$ , and  $\text{Er}^{3+}$  ions present as unintentional impurities

in the starting reagents, probably at ppm or sub-ppm concentration. We have shown that the intensities of these bands can be interpreted on the basis of the local structure of the cation sites in the ceria–zirconia solid solutions as obtained from crystallographic investigations. The lanthanide ions present as impurities can therefore be considered as useful spectroscopic probes of the site symmetry of the metal ions. In fact, their very low concentration makes them ideal probes, as it prevents unwanted effects, such as distortion of the host lattice, formation of clusters, inhomogeneous broadening, and luminescence quenching through cross-relaxation processes. Trivalent lanthanide luminescence transitions also appear to be present for wavenumbers lower than 800  $\text{cm}^{-1}$  from the laser excitation line, that is, in the spectral region usually associated only with Raman bands. For this reason we point out that structural information obtained exclusively from the analysis of Raman spectra measured only with one laser line could be flawed by the presence of impurity emissions bands.

**Acknowledgment.** University of Trieste, University of Verona, Regione Friuli Venezia Giulia, MURST–PRIN 2001 Contract No. 2001035514\_001 and PRIN 2002 Contract No. 2002034739\_005, FIRB2001 Contract No. RBNE0155X7, Center of Excellence for Nanostructured Materials, University of Trieste, are acknowledged for financial support. The authors thank Erica Viviani (University of Verona) for expert technical assistance.

CM035370B

(55) Luo, M. F.; Lu, G. L.; Zheng, X. M.; Zhong, Y. J.; Wu, T. H. *J. Mater. Sci. Lett.* **1998**, *17*, 1553.

(56) Trovarelli, A.; Zamar, F.; Llorca, J.; de Leitenburg, C.; Dolcetti, G.; Kiss, J. T. *J. Catal.* **1997**, *169*, 490.

(57) Zhao, X. Y.; Vanderbilt, D. *Phys. Rev. B* **2002**, *6507*, 5105.